energies

MDPI

Article

A Novel Temperature-Independent Model for Estimating the Cooling Energy in Residential Homes for Pre-Cooling and Solar Pre-Cooling

Simon Heslop [1], Baran Yildiz [1], Mike Roberts [1], Dong Chen [2], Tim Lau [3], Shayan Naderi [4], Anna Bruce [1,*], Iain MacGill [5] and Renate Egan [1]

[1] School of Photovoltaic and Renewable Energy Engineering, University of New South Wales, Sydney, NSW 2052, Australia
[2] The Commonwealth Scientific and Industrial Research Organisation, Melbourne, VIC 3190, Australia
[3] UniSA STEM, University of South Australia, Adelaide, SA 5095, Australia
[4] School of Built Environment, University of New South Wales, Sydney, NSW 2052, Australia
[5] School of Electrical Engineering and Telecommunications, University of New South Wales, Sydney, NSW 2052, Australia
* Correspondence: a.bruce@unsw.edu.au

Abstract: Australia's electricity networks are experiencing low demand during the day due to excessive residential solar export and high demand during the evening on days of extreme temperature due to high air conditioning use. Pre-cooling and solar pre-cooling are demand-side management strategies with the potential to address both these issues. However, there remains a lack of comprehensive studies into the potential of pre-cooling and solar pre-cooling due to a lack of data. In Australia, however, extensive datasets of household energy measurements, including consumption and generation from rooftop solar, obtained through retailer-owned smart meters and household-owned third-party monitoring devices, are now becoming available. However, models presented in the literature which could be used to simulate the cooling energy in residential homes are temperature-based, requiring indoor temperature as an input. Temperature-based models are, therefore, precluded from being able to use these newly available and extensive energy-based datasets, and there is a need for the development of new energy-based simulation tools. To address this gap, a novel data-driven model to estimate the cooling energy in residential homes is proposed. The model is temperature-independent, requiring only energy-based datasets for input. The proposed model was derived by an analysis comparing the internal free-running and air conditioned temperature data and the air conditioning data for template residential homes generated by AccuRate, a building energy simulation tool. The model is comprised of four linear equations, where their respective slope intercepts represent a thermal efficiency metric of a thermal zone in the template residential home. The model can be used to estimate the difference between the internal free-running, and air conditioned temperature, which is equivalent to the cooling energy in the thermal zone. Error testing of the model compared the difference between the estimated and AccuRate air conditioned temperature and gave average CV-RMSE and MAE values of 22% and 0.3 °C, respectively. The significance of the model is that the slope intercepts for a template home can be applied to an actual residential home with equivalent thermal efficiency, and a pre-cooling or solar pre-cooling analysis is undertaken using the model in combination with the home's energy-based dataset. The model is, therefore, able to utilise the newly available extensive energy-based datasets for comprehensive studies on pre-cooling and solar pre-cooling of residential homes.

Keywords: pre-cooling; solar pre-cooling; air conditioning; demand side management; solar self-consumption

Citation: Heslop, S.; Yildiz, B.; Roberts, M.; Chen, D.; Lau, T.; Naderi, S.; Bruce, A.; MacGill, I.; Egan, R. A Novel Temperature-Independent Model for Estimating the Cooling Energy in Residential Homes for Pre-Cooling and Solar Pre-Cooling. *Energies* **2022**, *15*, 9257. https://doi.org/10.3390/en15239257

Academic Editor: Carla Montagud

Received: 31 October 2022
Accepted: 2 December 2022
Published: 6 December 2022

1. Introduction

The global solar photovoltaic (PV) market has experienced exceptional growth over the last 10 years, with annual installations increasing from under 10 GWp in 2009 to nearly 120 GWp at the end of 2019 [1]. As of 2019, Australia had the second highest solar penetration levels per capita in the world [1]. The increase in solar has contributed to a change in the Australian National Electricity Market (NEM) generation mix through a reduction in conventional synchronous generation. According to the Australian Energy Market Operator (AEMO), this change has reduced grid flexibility and system inertia, putting system security at risk [2]. In the AEMO Renewable Integration Study [3], key challenges listed include how to manage NEM contingency and system dispatchability with increasing solar penetration levels. The impacts are also being felt at the distribution level [4]. Attempts to manage the negative impact of elevated levels of solar penetration in Australia provide an interesting and valuable case study that is relevant to other jurisdictions experiencing high and increasing penetrations of solar.

Flexible demand, through demand-side management (DSM), is one way to increase grid flexibility in a high solar penetration environment [5]. DSM involves shifting the time that flexible loads, such as electric hot water (EHW) systems, batteries, and air conditioning units (AC), are operated. In Australia, AC DSM is a suitable candidate for increasing grid flexibility, as peak demand occurs during summer and winter due to large AC consumption. For example, in South Australia on a typical hot summer day, AC and refrigeration systems consume 46% of the state's total produced electricity [4]. Due to the importance of providing flexible demand through AC DSM, the Australian Renewable Energy Agency (ARENA), a government organisation tasked with funding projects to promote renewable energy, has sponsored a number of AC DSM pilot projects and trials [6].

Pre-cooling (PC) is a form of DSM where the AC unit cools the thermal mass of a building prior to the time when space cooling would normally occur [7]. Solar pre-cooling (SPC) is as per PC but where excess solar export is used to power the AC unit. The space cooling energy required later is then reduced by the residual energy in the thermal mass. Both PC and SPC typically shift AC demand towards the middle of the day and, therefore, have the potential to mitigate the excessive reduction in net demand caused by excessive residential solar export during the day and reduce evening peak demand on days of extreme temperature due to excessive AC consumption. Furthermore, SPC has the potential to reduce household electricity costs through tariff arbitrage [8].

1.1. Existing Research on Pre-Cooling

A heavily cited paper [9] describes a pre-cooling control strategy designed to limit the peak cooling load of a commercial building to 75% of the capacity of existing cooling equipment (one chiller) with minimal impact on occupant comfort. Results show the control strategy successfully limited the maximum cooling demand while maintaining comfort levels, providing an alternative to the installation of a second chiller. Other studies describe pre-cooling strategies for commercial buildings [10–15], while [16] examines pre-cooling for residential buildings. In [16], the residential building simulation tool, REGCAP, was used to investigate peak cooling energy demand reduction through pre-cooling. Results showed that peak cooling demand was reduced by at least 50%, but at the expense of an overall increase (up to 67%) in cooling energy consumption. It was also found that the amount of cooling energy that can be shifted is heavily dependent on the climate zone, the length of the pre-cooling period, and the pre-cooling set point. In [17], a number of pre-cooling strategies, which combined a range of temperature setpoints and pre-cooling durations, were tested for five households. Savings are made through tariff arbitrage, and a reduction in electricity costs of up to 8.5% was achieved over the period simulated. Ref. [18] It was also found that peak reduction is achievable through pre-cooling, with results showing that pre-cooling for 1 h before the peak demand period and increasing the thermostat by just two degrees can reduce peak AC demand by 68%.

1.2. Existing Research on Solar Pre-Cooling

Existing work examining solar pre-cooling include [19], where solar generation and AC consumption in buildings are optimised to minimise the cost of electricity while minimising discomfort levels. SPC is included in one of the optimisation strategies and simulated to occur one hour before predicted occupancy. Results show that SPC results in greater comfort levels, but at the expense of more energy employed overall.

In [20], the authors extend the U.S. National Renewable Energy Laboratory's Renewable Energy Optimization (REopt) model to include a control strategy called "solar plus", utilising the simulation tool EnergyPlus, in which both EHW and AC systems are controlled. A form of SPC, called drifting, is included in the model. Drifting maintains household temperature within an expanded temperature dead band, resulting in reduced AC consumption overall. A net present value (NPV) analysis is conducted for a variety of tariffs and finds that solar plus results in a better financial outcome in all cases.

In [21], optimisation of SPC combined with Thermal Energy Storage (TES) aimed to reduce both peak demand and the cost of electricity. The TES was modelled to be similar to the Ice Bear technology [22]. On the hottest day simulated, the combined SPC and TES strategies resulted in a peak demand reduction of up to 75.6%. In [23], to reduce reliance on diesel generation during power outages, the authors propose a look-ahead optimisation framework that uses solar and batteries for pre-cooling. The framework is designed for commercial buildings in developing countries, and results show that it can reduce diesel fuel consumption by up to 42%. In [24], the authors use simulation modelling and experimental measurements to examine the feasibility of using solar pre-cooling to flatten residential net demand in three homes in Phoenix, AZ, USA. Results show that annual savings of up to USD 160 for homeowners are possible. It was also found that net demand variability due to solar generation can be reduced by up to 90%. In [25], the authors proposed five different control strategies to shift the peak demand of a solar PV system integrated heat pump that supplies a radiant wall. One control strategy, termed Solar Predictive, uses SPC, where the temperature setpoint to be obtained through solar pre-cooling in the morning is determined by the forecasted daytime temperatures. The case study is a simple cubicle, modelled using a six-surface star network according to the methodology proposed in [26]. Results for Solar Predictive control show that pre-cooling the radiant wall increases the overall energy consumed by the heat pump but reduces peak demand. Related work by the same authors [27] found that an optimised SPC strategy is more cost-effective than installing more solar PV capacity without any control strategy.

In [28], the authors investigated how solar pre-cooling can be used to "flatten the duck curve" or increase minimum daytime demand due to excessive solar PV export. The Smart Residential Load Simulator [29] was used to simulate solar pre-cooling scenarios. Results of simulations show that the change in aggregated load profile from solar pre-cooling will increase minimum demand for a case study in California, but only for certain solar PV penetration levels. An economic analysis using existing time-of-use tariffs was also presented and showed that additional incentives would be necessary to motivate households to adopt solar pre-cooling. The potential collective savings and peak reduction through SPC for a collection of buildings, both residential and commercial, is also examined in [30,31].

1.3. Paper Contribution

A review of the literature indicates that there remains a lack of comprehensive studies into the potential of PC and SPC for typical residential homes, considering different building types, occupancy behaviour, and weather conditions, primarily due to the lack of available household data. Recently, however, extensive, energy-based residential datasets obtained through retailer-owned smart meters and household-owned third-party monitoring devices are now becoming available in Australia. However, the models presented in the literature, which could be used to simulate the cooling energy in residential homes, are temperature-based, requiring indoor temperature as an input. These temperature-based models are,

therefore, precluded from being able to make use of the recently available energy-based datasets, and there is a need for the development of new energy-based simulation tools which can. To address this gap, a novel data-driven model to estimate the cooling energy in residential homes is proposed. The model is temperature-independent, requiring only energy-based datasets as input.

The proposed model was derived through analysis comparing the internal free-running and air conditioned temperature data, and the air conditioning data for template residential homes generated by AccuRate, an established and validated building energy simulation tool. The model is comprised of four linear equations, where their respective slope intercepts represent a thermal efficiency metric of a thermal zone in the template residential home. The model can be used to estimate the difference between the internal free-running and air conditioned temperature, which is equivalent to the cooling energy in the thermal zone.

Error testing of the model compared the difference between the estimated and AccuRate air conditioned temperature and gives average CV-RMSE and MAE values of 22% and 0.3 °C, respectively. The CV-RMSE value for all template homes is less than 30%, the minimum level of accuracy for a data-driven model accepted by The American Society of Heating, Refrigerating, and Air-Conditioning Engineers (ASHRAE).

The significance of the model is that the thermal efficiency metrics for a template home can be applied to an actual residential home with equivalent thermal efficiency. A pre-cooling or solar pre-cooling analysis can then be undertaken for the residential home using the model in combination with its associated energy-based dataset. The model is, therefore, able to utilise the newly available extensive energy-based datasets for comprehensive studies on pre-cooling and solar pre-cooling of residential homes.

The paper is structured as follows. Section 2 describes the software tool AccuRate, Section 3 describes the method, Section 4 presents the results, Section 5 describes the significance of the model, and Section 6 provides concluding comments.

2. AccuRate

AccuRate [32] is a dynamic building energy simulation tool developed by the Commonwealth Scientific and Industrial Research Organisation (CSIRO), which is commonly used to rate the energy efficiency of houses, according to the Australian Nationwide House Energy Rating Scheme (NatHERS) [33]. AccuRate estimates the AC energy consumption and indoor temperatures on an hourly basis for a building based on user-defined inputs of building material, geometry, weather data, and the design of the AC system. AccuRate has previously been validated [34] using the well-established BESTEST protocol [35] developed by the National Renewable Energy Laboratory (NREL) in conjunction with the International Energy Agency. The validation process involves running the AccuRate simulation tool under prescribed, but varied, conditions, and comparing the results against other well-established models. The validation process showed that AccuRate was able to predict peak heating demand and peak cooling demand to within ≈1.8% and ≈9.3%, respectively. The results are within the range of the reference simulation tools' predictions. The simulated measurements generated by AccuRate are, therefore, considered to be sufficiently dependable for use in this study.

The simulated measurements generated by AccuRate for the buildings used in this study include the following:

- T_{FR} (°C) is the free running temperature, i.e., the indoor temperature with no AC;
- T_{AC} (°C) is the air conditioned temperature, i.e., the indoor temperature where AC is controlled to maintain thermal comfort using a temperature setpoint; and
- EE_{in} (kWh) is the electrical energy consumed by the AC unit.

Twenty-four template homes were created using AccuRate, consisting of six build types for four Australian eastern capital cities, namely Brisbane, Sydney, Melbourne, and Adelaide. Build type is classified by construction weight (heavy, medium, and light) and its star rating (2-star and 6-star). The star rating of a home is based on NatHERS, which

assigns a 0- to 10-star rating to a home according to its thermal comfort and energy efficiency. According to [36], 2-star homes make up the majority (72%) of Australian homes, and 6-star is the current build standard. Construction materials were selected to attain the three different build weights, and two different star ratings for each build weight for all four cities, whereas construction materials selected differed according to the climate of each city and the desired star rating. Table 1 gives the construction details for each template home. Three months' (covering a summer) worth of simulated temperature measurements (T_{FR}, T_{AC}) and air conditioning data (EE_{in}) were generated for each template home for four bedrooms (thermal zones). Assumed occupancy profiles, thermostat settings, and window, curtain, and external shading operations used by AccuRate when generating the simulated measurements are given in [37], Appendix B.

Table 1. Build characteristics for the twenty-four template homes created in AccuRate. Rx = the R-value of the construction material (K.m^2/W), SG = Single glazing and DG = Double glazing.

Template Home	City	Climate	Build Type		Walls	Windows	Floors	Ceilings
			Star Rating	Build Weight				
B2L	Brisbane	Humid Subtropical	2	Light	R0	SG	R0	R0
B2M				Medium	R0	SG	R0	R0.1
B2H				Heavy	R0	SG	R0	R0.4
B6L			6	Light	R0	SG	R0	R4
B6M				Medium	R0.7	DG	R0	R4
B6H				Heavy	R2.3	DG	R2.5	R5
S2L	Sydney	Humid Subtropical	2	Light	R0	SG	R0	R0
S2M				Medium	R0	SG	R0	R0
S2H				Heavy	R0	SG	R0	R0.5
S6L			6	Light	R1.3	SG	R0	R4
S6M				Medium	R0.9	DG	R0	R4
S6H				Heavy	R2.5	DG	R3	R5
M2L	Melbourne	Temperate	2	Light	R0	SG	R0	R0.1
M2M				Medium	R0	SG	R0	R0.1
M2H				Heavy	R0	SG	R0	R0
M6L			6	Light	R2	SG	R0	R4
M6M				Medium	R1.1	DG	R0	R4
M6H				Heavy	R1.4	DG	R3	R4
A2L	Adelaide	Mediterranean	2	Light	R0	SG	R0	R0
A2M				Medium	R0	SG	R0	R0.1
A2H				Heavy	R0	SG	R0	R0.3
A6L			6	Light	R0.4	SG	R0	R2.5
A6M				Medium	R0.7	DG	R0	R4
A6H				Heavy	R2	DG	R3	R4

3. Method

This section presents the temperature-independent model for estimating the cooling energy present in a thermal zone. Analysis was conducted comparing AccuRate variables T_{FR}, T_{AC}, and EE_{in}, and resulted in the derivation of four linear equations, where their

respective slope intercepts represent a thermal efficiency metric of a thermal zone in the template residential home.

Each linear equation is constituted by a combination of EE_{in} and two derived variables: T_{in} and T_{tm}. Where T_{in} represents the temperature difference due to cooling energy injected into the thermal zone by the AC unit and T_{tm} represents the temperature difference due to the cooling energy stored in the thermal mass.

The model can be used to estimate the difference between T_{FR} and T_{AC}, defined as T_{FRAC}, which is equivalent to the cooling energy in the thermal zone.

To give a graphical illustration of the relationship between temperature variables T_{FR}, T_{AC}, T_{in}, and T_{tm}, a time-series (hourly) plot illustrating their typical behaviour during the cooling period is presented in Figure 1. The cooling period consists of two phases, the charging phase and the discharging phase, where h_{ch} is the first hour of the charging phase and h_{dc} is the first hour of the discharging phase. During the charging phase, electrical energy (EE_{in}) is consumed by the AC unit and cooling energy is injected into the thermal zone. During the discharging phase, no new cooling energy is injected and T_{tm} decays over time. T_{in} is represented by the green arrows and T_{tm} by the orange bars.

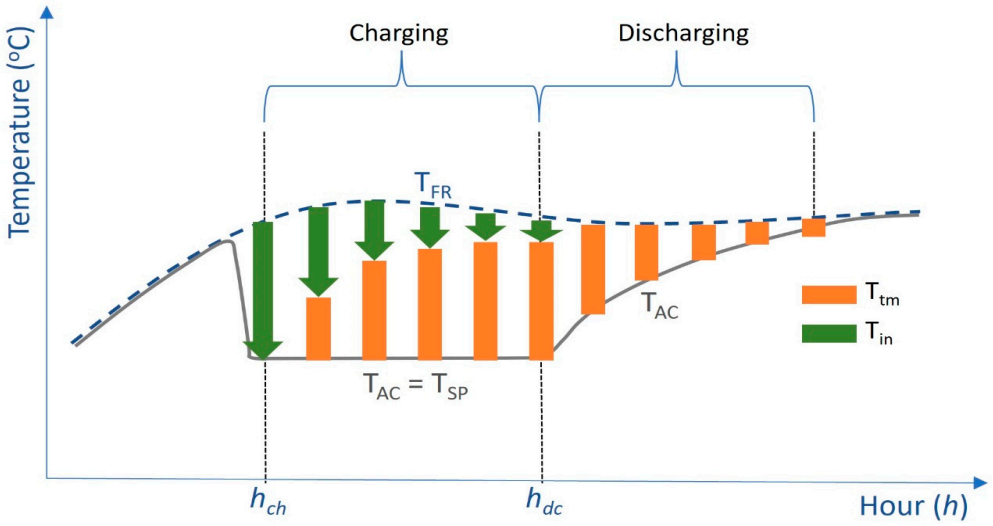

Figure 1. Time-series plot illustrating the typical behaviour of temperatures T_{FR}, T_{AC}, T_{tm}, and T_{in} during the charging and discharging phase.

3.1. Linear Equations

The four linear equations are defined in this section. The linear equations are introduced and referred to by the thermal efficiency metric that their respective slope-intercept represents. The four thermal efficiency metrics are the AC cooling efficiency (e), the thermal mass charging rate (c), the thermal mass fast discharging rate (d^F), and the thermal mass slow discharging rate (d^S).

AC cooling efficiency (e). There is a linear relationship at $h = h_{ch}$ between EE_{in} and T_{in}, as defined by Equation (1):

$$T_{in}[h] = e_m \times CoP \times EE_{in}[h] + e_i, \ for\ h = h_{ch} \quad (1)$$

where e_m and e_i are the slope and intercept, respectively, of the AC cooling efficiency (e), CoP is the coefficient of performance of the AC unit, and h is the hour. As $T_{in} = T_{FRAC}$ at $h = h_{ch}$, this linear relationship indicates that T_{FRAC} is a measure of the cooling energy in the thermal zone. The average R^2 value of this linear relationship for all template homes is 0.93. Table A2 in Appendix A gives the AC cooling efficiency R^2 values for all template homes. As an example, Figure 2 gives the scatter plot of EE_{in} versus T_{in} for Bedroom 1 in template home M2L.

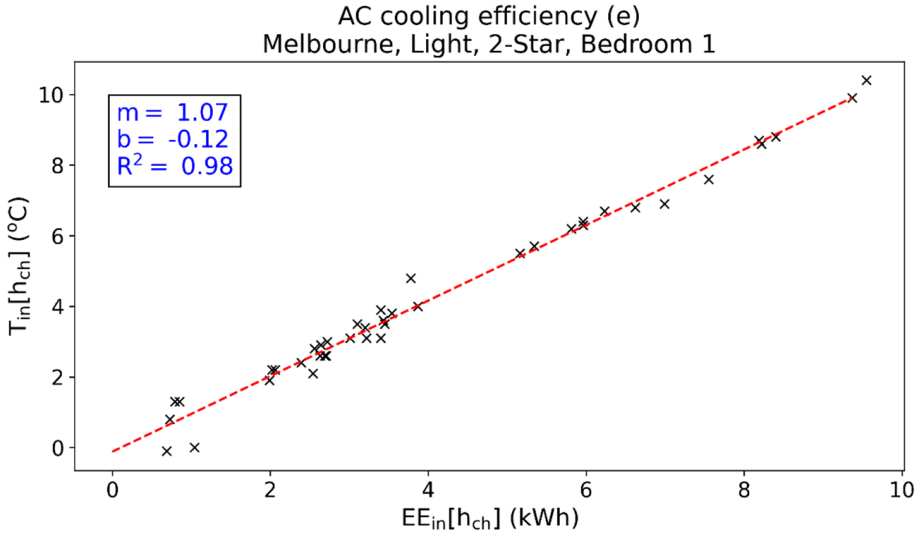

Figure 2. Scatter plot of $EE_{in}[h_{ch}]$ versus $T_{in}[h_{ch}]$, defining the AC cooling efficiency (e) for Bedroom 1 in template home M2L.

Thermal mass charging rate (c). There is a second linear relationship at $h = h_{ch}$ between T_{in} and T_{tm}, as defined by Equation (2):

$$T_{tm}[h+1] = c_m \times T_{in}[h] + c_i, \ for\ h = h_{ch} \quad (2)$$

where c_m and c_i are the slope and intercept, respectively, of the thermal mass charging rate (c). Equation (2) represents the rate in which the thermal mass is charged with cooling energy. The average R^2 value of this linear relationship for all template homes is 0.9. Table A3 in Appendix A gives the thermal mass charging rate R^2 values for all template homes. As an example, Figure 3 gives the scatter plot of $T_{in}[h_{ch}]$ versus $T_{tm}[h_{ch} + 1]$ for Bedroom 1 in template home M2L.

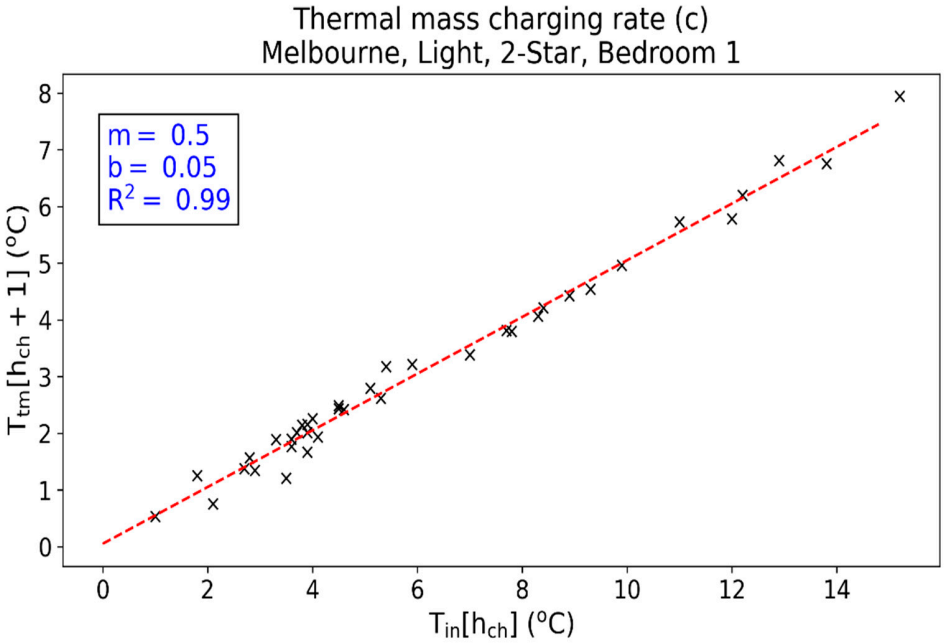

Figure 3. Scatter plot of $T_{in}[h_{ch}]$ versus $T_{tm}[h_{ch} + 1]$, defining the thermal mass charging rate (c) for Bedroom 1 in template home M2L.

Thermal mass fast discharging rate (d^F). There is a linear relationship at $h = h_{dc}$ between T_{FRAC} and T_{tm}, as defined by Equation (3):

$$T_{tm}[h+1] = d_m^F \times T_{FRAC}[h] + d_i^F, \; for \; h = h_{dc} \tag{3}$$

where and d_m^F and d_i^F are the slope and intercept, respectively, of the thermal mass fast discharging rate (d^F). Equation (3) represents the rate at which cooling energy is discharged from the thermal mass at $h = h_{dc}$. The average R^2 value of this linear relationship for all template homes is 0.91. Table A4 in Appendix A gives the thermal mass fast discharging rate R^2 values for all template homes. As an example, Figure 4 gives the scatter plot of $T_{FRAC}[h_{dc}]$ versus $T_{tm}[h_{dc} + 1]$ for Bedroom 1 in template home M2L.

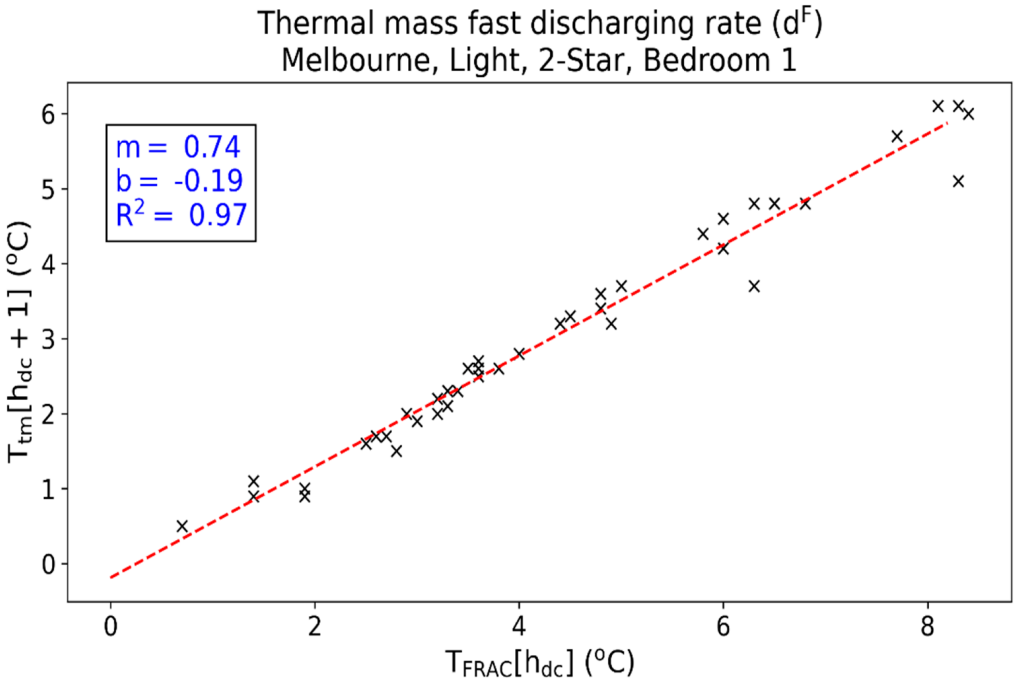

Figure 4. Scatter plot of $T_{FRAC}[h_{dc}]$ versus $T_{tm}[h_{dc} + 1]$, defining the thermal mass fast charging rate d^F, for Bedroom 1 in template home M2L.

Thermal mass slow discharging rate (d^S). There is a linear relationship for $h > h_{dc}$ between $T_{tm}[h + 1]$ and $T_{tm}[h]$, as defined by Equation (4):

$$T_{tm}[h+1] = d_m^S \times T_{tm}[h] + d_i^S, \; for \; h > h_{dc} \tag{4}$$

where d_m^S and d_i^S are the slope and intercept, respectively, of the thermal mass slow discharging rate (d^S). Equation (4) represents the rate at which cooling energy is discharged from the thermal mass for $h > h_{dc}$. The average R^2 value of this linear relationship for all template homes is 0.99. Table A5 in Appendix A gives the thermal mass slow discharging rate R^2 values for all template homes. As an example, Figure 5 gives the scatter plot of $T_{tm}[h]$ versus $T_{tm}[h + 1]$ for $h > h_{dc}$ for Bedroom 1 in template home M2L.

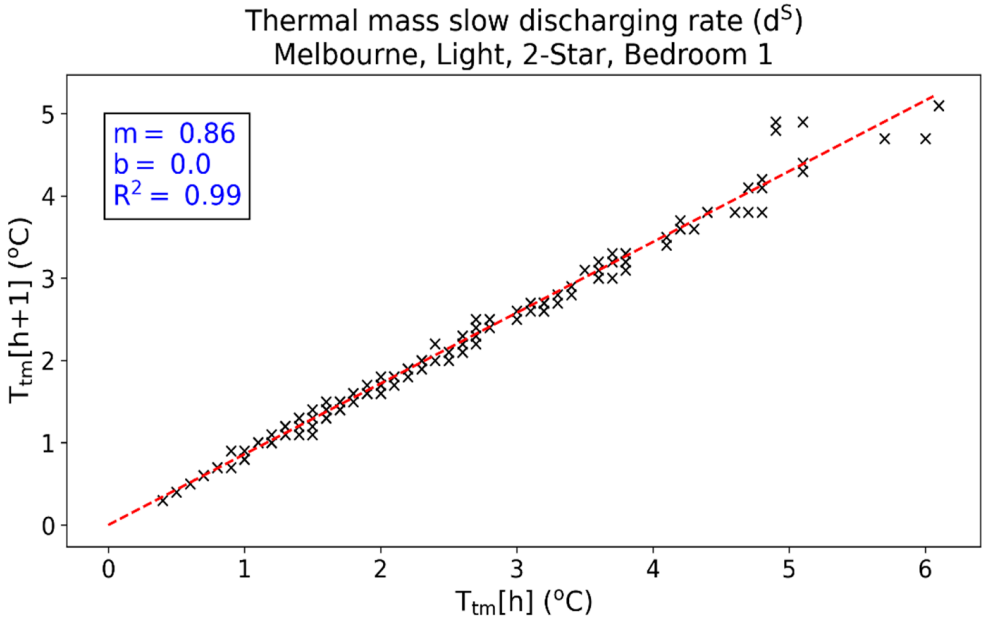

Figure 5. Scatter plot of $T_{tm}[h]$ versus $T_{tm}[h+1]$ for $h > h_{dc}$, defining the thermal mass slow charging rate d^S for Bedroom 1 in template home M2L.

Why a fast and a slow discharging rate? According to [38], the rate of change of the temperature in a thermal zone after a heater has been turned off changes, becoming slower with time. To ensure that this thermal behaviour was captured by the model, the thermal mass discharging rate at each hour following h_{dc} was calculated. It was discovered that the discharging rate for the first hour was clearly faster than later hours, but then remained relatively unchanged, similar to what was discovered in [38]. Therefore, it was decided that two rates, one for the first hour (fast), and a second for the hours following (slow), were sufficient to accurately model thermal discharging.

3.2. Implementation of the Model

Implementation of the model consists of the following operational assumptions.

(1) The sum of T_{in} and T_{tm} equals T_{FRAC}, as defined by Equation (5):

$$T_{FRAC} = T_{in} + T_{tm} \tag{5}$$

(2) Equation (1) can be used to calculate T_{in} at any hour h.

(3) During the charging phase, the thermal dynamics of the home are assumed to operate in accordance with Equation (6):

$$T_{tm}[h+1] = \{c_m \times T_{in}[h] + c_i\} + \left\{d_m^F \times T_{tm}[h] + d_i^F\right\} \tag{6}$$

where Equation (6) represents the assumption that during the charging phase, the cooling energy stored in the thermal mass consists of new charging energy (due to EE_{in} from the previous hour) and undischarged energy preserved in the thermal mass from the previous hour.

Equations (1)–(6) can be used to calculate T_{tm} and T_{FRAC} at any hour of the charging or discharging phase. A flowchart describing the process for implementing the model is given in Figure 6. The flowchart shows that EE_{in} is the only input from the AccuRate dataset used to implement the model. Neither T_{FR} nor T_{AC} are required, which is evidence that the model is temperature-independent.

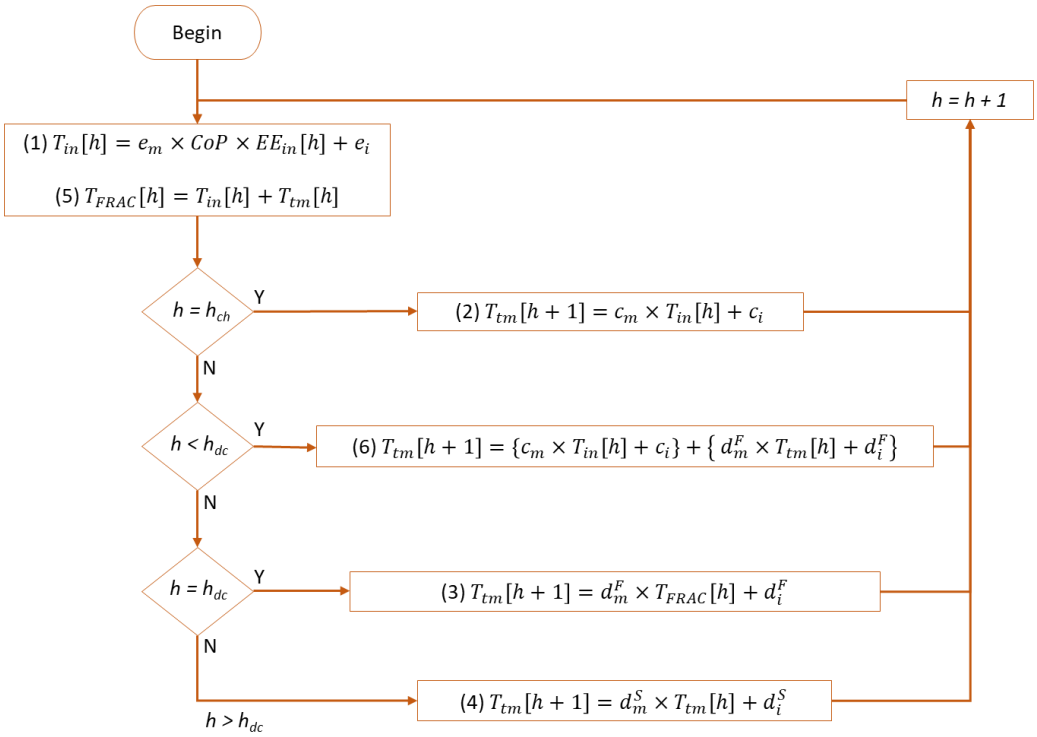

Figure 6. Flowchart describing the process for implementing the model.

4. Results

The accuracy of the model is tested by calculating the average Coefficient of Variation of Root-Mean Squared Error (CV-RMSE) and Mean Absolute Error (MAE) of the difference between the air conditioning temperature, estimated by the model (eT_{AC}), and the AccuRate air conditioning temperature (T_{AC}) during the charging and discharging period for 15 of the 24 template homes, where eT_{AC} is calculated using Equation (7):

$$eT_{AC} = T_{FR} - eT_{FRAC} \quad (7)$$

where eT_{FRAC} is calculated using the process described in the flowchart in Figure 6.

Nine homes were excluded as there was insufficient data (less than 10 air conditioning days) to determine the thermal metrics. Results are given in Table 2 and show that the average CV-RMSE and MAE values are 22% and 0.3 °C, respectively. Unfortunately, to the authors' best knowledge, there are no equivalent studies to compare these results against. However, ASHRAE gives guidance in [39], where it is specified that for data-driven models, CV-RMSE is the recommended error estimation method, and 30% CV-RMSE is the minimum acceptable level of accuracy. The CV-RMSE value for the fifteen template homes is less than 30%, indicating that the model is sufficiently accurate according to ASHRAE.

Figure 7 gives the time series of the free-running temperature (T_{FR}), air conditioned temperature (T_{AC}), and the estimated air conditioned temperature (eT_{AC}) for the first four days for template home M2L. The light orange boxes highlight the periods of charging and discharging, which is also the period over which the CV-RMSE and MAE are calculated. The MAE during the charging and discharging periods is less than 0.5 °C at all hours, demonstrating the accuracy of the proposed model.

Table 2. CV-RMSE and MAE for 15 of 24 template homes.

Template Home	City	CV-RMSE (%)	MAE (°C)	Air Conditioning Days
B2L	Brisbane	19.18	0.21	63
B2M		19.74	0.22	62
B2H		22.08	0.24	91
B6L		14.99	0.15	29
B6M		22.33	0.21	52
B6H		N/A	N/A	3
S2L	Sydney	20.43	0.25	21
S2M		21.91	0.23	27
S2H		N/A	N/A	8
S6L		N/A	N/A	7
S6M		21.82	0.25	15
S6H		N/A	N/A	5
M2L	Melbourne	23.1	0.3	13
M2M		16.76	0.28	13
M2H		N/A	N/A	3
M6L		18.79	0.31	12
M6M		N/A	N/A	5
M6H		N/A	N/A	2
A2L	Adelaide	26.53	0.44	20
A2M		25.77	0.43	24
A2H		N/A	N/A	7
A6L		28.12	0.57	12
A6M		26.65	0.42	18
A6H		N/A	N/A	8

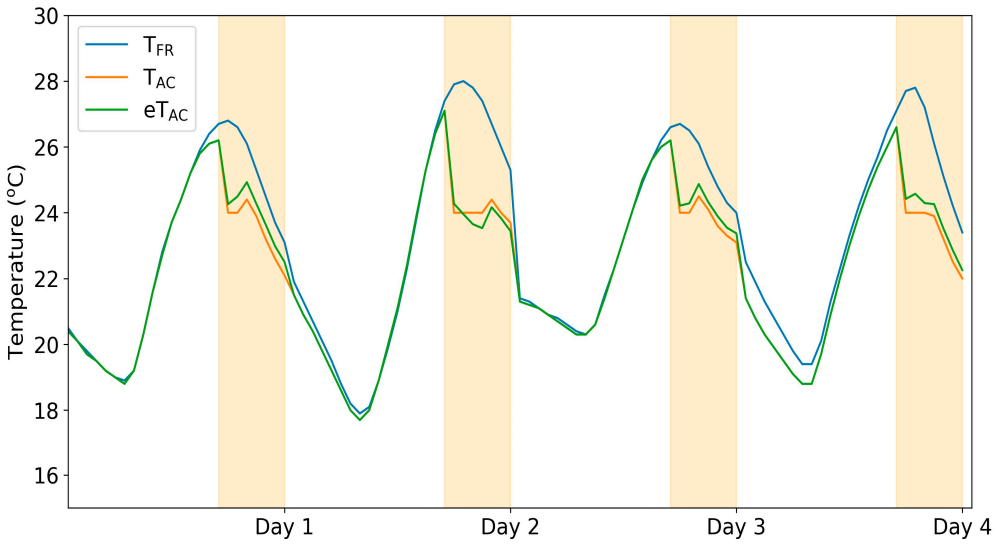

Figure 7. Time series of the free-running temperature (T_{FR}), air conditioned temperature (T_{AC}), and the estimated air conditioned temperature (eT_{AC}) for four days for template home M2L. The light orange boxes highlight the periods of charging and discharging.

5. Model Significance

By applying the thermal efficiency metrics for a template home to an actual residential home with an equivalent thermal efficiency, a pre-cooling and solar pre-cooling analysis can then be undertaken for the residential home using the model in combination with its associated energy-based dataset. This is significant as the model can, therefore, make use of the newly available extensive energy-based datasets for comprehensive studies on pre-cooling and solar pre-cooling for residential homes.

For example, since ~72% of Australian homes are estimated to be 2-star [36], the thermal efficiency metrics for a template residential home with a 2-star rating could be applied to these homes, and a pre-cooling or solar pre-cooling analysis could be undertaken for each, using the proposed model in combination with their associated energy-based datasets. An example to demonstrate how the model can be used to simulate solar pre-cooling is given in Appendix A.

Other dynamic building energy simulation tools (such as EnergyPlus) could also be used to generate the thermal efficiency metrics for a "typical" residential building, and the proposed model could then be implemented to undertake a pre-cooling or solar pre-cooling analysis for that type of building.

6. Conclusions

The paper proposes a novel data-driven model to estimate the cooling energy in residential homes. The model is temperature-independent, requiring only energy-based datasets as input. The proposed model was derived through analysis comparing the internal free-running and air conditioned temperature data, and the air conditioning data for template residential homes generated by AccuRate, an established and validated building energy simulation tool.

Error testing of the model comparing the difference between the estimated and AccuRate air conditioned temperature gives average CV-RMSE and MAE values of 22% and 0.3 °C, respectively. The CV-RMSE value for all template homes is less than 30%, the minimum level of accuracy for a data-driven model accepted by ASHRAE.

The significance of the model is that the thermal efficiency metrics for a template home can be applied to an actual residential home with equivalent thermal efficiency. A pre-cooling or solar pre-cooling analysis can then be undertaken for the residential home using the model in combination with an energy-based dataset. The model is, therefore, able to utilise the newly available extensive energy-based datasets for comprehensive studies on pre-cooling and solar pre-cooling of residential homes.

Potential future work includes:

- Extending the model to solar pre-heating;
- An analysis of the potential of solar pre-cooling using measured residential energy data to examine the impact of build type, climate, and different solar pre-cooling control and optimisation algorithms to reduce peak demand, increase minimum demand, and reduce electricity costs;
- The development of proof to explain the strong R^2 values for the thermal metrics; and
- The development of a model to derive the thermal metrics of a building from its energy data.

Supplementary Materials: The following supporting information can be downloaded at: https://www.mdpi.com/article/10.3390/en15239257/s1.

Author Contributions: Conceptualization, S.H.; Methodology, S.H., T.L. and S.N.; Software, S.H.; Validation, S.H. and M.R.; Formal analysis, S.H.; Investigation, S.H.; Data curation, D.C.; Writing—original draft, S.H.; Writing—review & editing, B.Y., M.R., D.C., T.L., S.N., A.B., I.M. and R.E.; Visualization, B.Y. and S.N.; Supervision, A.B. and I.M. All authors have read and agreed to the published version of the manuscript.

Funding: This research received grant funding from the Australian Government through the Co-operative Research Centre Projects program (CRC-P). This article was an invited paper for Special Issue entitled "Energy Efficiency and Optimization Strategies in Buildings for a Sustainable Future", and the APC charge was waived.

Data Availability Statement: The AccuRate data used in this study is available as a zip file, AccuRate data.zip from Supplementary Materials.

Acknowledgments: The authors acknowledge the data provided for research purposes by AccuRate.

Conflicts of Interest: The authors declare no conflict of interest.

Nomenclature

c	is the thermal mass charging rate
c_m	is the slope of the thermal mass charging rate (c)
c_i (°C)	is the intercept of the thermal mass charging rate (c)
CoP	is the coefficient of performance of the AC unit
$CV\text{-}RMSE$ (%)	is the Coefficient of the Variation of the Root Mean Square Error
d^F	is the thermal mass fast discharging rate
d^F_m	is the slope of the thermal mass fast discharging rate (d^F)
d^F_i (°C)	is the intercept of the thermal mass fast discharging rate (d^F)
d^S	is the thermal mass slow charging rate
d^S_m	is the slope of the thermal mass slow discharging rate (d^S)
d^S_i (°C)	is the intercept of the thermal mass slow discharging rate (d^S)
e	is the AC cooling efficiency
e_m (°C/kWh)	is the slope of the AC cooling efficiency (e)
e_i (°C)	is the intercept of the AC cooling efficiency (e)
EE_{in} (kWh)	is the electrical energy consumed by the AC unit
EE^*_{in} (kWh)	is the equivalent electrical energy consumed by the AC unit to attain T_{tm}
h_{ch}	is the first hour of the charging phase
h_{dc}	is the first hour of the discharging phase
MAE (°C)	is the Mean Absolute Error
R^2	is the coefficient of determination
T_{AC} (°C)	is the air conditioned temperature.
T_{FR} (°C)	is the free running temperature, the indoor temperature with no air conditioning.
T_{FRAC} (°C)	is the difference between T_{FR} and T_{AC}.
T_{in} (°C)	represents the temperature difference due to cooling energy injected into the thermal zone by the AC unit
T_{tm} (°C)	represents the temperature difference due to the cooling energy stored in the thermal mass

Appendix A

Solar Pre-Cooling Example

An example to demonstrate how the model can be used to simulate solar pre-cooling is given in this section. Figure A1a,b illustrate the example. Figure A1a shows an example scenario where excess solar energy (EE_{solar}) at hours h_{ch} = 13 and h_{dc} = 14 is diverted to the AC unit (EE_{in}). In this scenario, the existing (peak) AC consumption (EE_{peak}) at h = 16 is to be reduced through solar pre-cooling. Figure A1b shows the resultant calculated temperatures T_{tm}, T_{in}, and T_{peak}, where T_{peak} is the existing temperature due to EE_{peak}. In this example the home is assumed to have thermal metrics $e_m = CoP = 1$, $c_m = 0.5$, $d^F_m = 0.75$, $d^s_m = 0.85$, and $e_i = c_i = d^F_i = d^S_i = 0$. Table A1 gives the calculation of $T_{in}[h]$, $T_{tm}[h]$, $T_{FRAC}[h]$, and $T_{tm}[h+1]$ for the example, with the relevant equations also included.

At h = 16, the temperature difference due to the cooling energy stored in the thermal mass, T_{tm} = 3.2 °C, is deducted from T_{peak}. Re-arranging Equation (1), the reduction to EE_{peak} is calculated to be 3.2 kWh, where T_{tm} = 3.2 °C, $e_m = CoP = 1$ and $e_i = 0$. This example shows that no temperature inputs (T_{FR}, T_{AC}, or outdoor temperature) are required by the model to simulate solar pre-cooling.

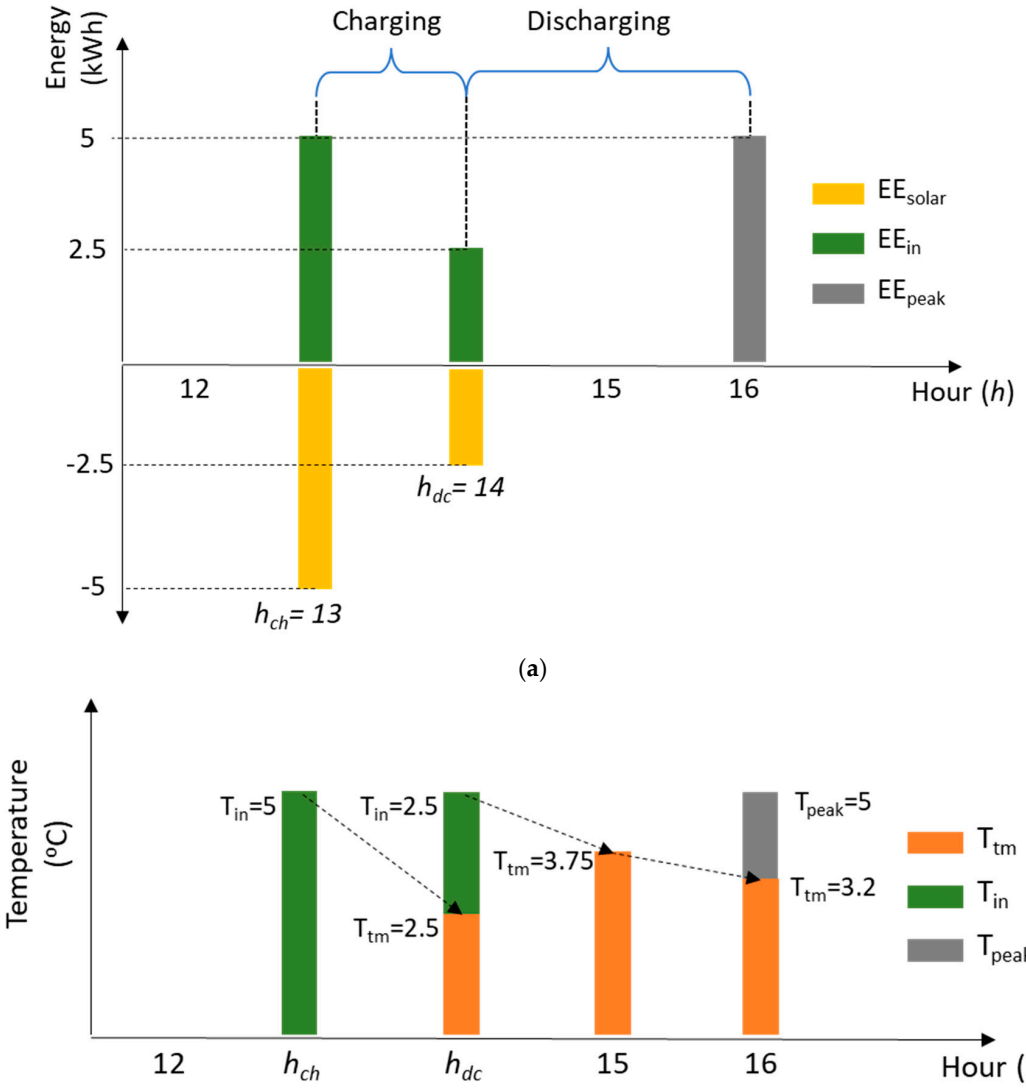

Figure A1. Illustration of example (**a**) gives the energy values (EE_{solar}, EE_{in}, and EE_{peak}) and (**b**) gives the temperature values (T_{in}, T_{tm}, and T_{peak}).

Table A1. Calculation of $T_{in}[h]$, $T_{tm}[h]$, $T_{FRAC}[h]$, and $T_{tm}[h+1]$ for the example; the equation used to make each calculation is included.

	$h = h_{ch}$	$h = h_{dc}$
$T_{in}[h]$	(1) $e_m \times CoP \times EE_{in}[h] = 5$	(1) $e_m \times CoP \times EE_{in}[h] = 2.5$
$T_{tm}[h]$	0	2.5
$T_{FRAC}[h]$	(5) $T_{in}[h] + T_{tm}[h] = 5$	(5) $T_{in}[h] + T_{tm}[h] = 5$
$T_{tm}[h+1]$	(6) $c_m \times T_{in}[h] + d_m^f \times T_{tm}[h] = 2.5$	(3) $d_m^f \times T_{FRAC}[h] = 3.75$
	$h = 15$	$h = 16$
$T_{in}[h]$	0	0
$T_{tm}[h]$	3.75	3.2
$T_{FRAC}[h]$	(5) $T_{in}[h] + T_{tm}[h] = 3.75$	
$T_{tm}[h+1]$	(4) $d_m^s \times T_{tm}[h] = 3.2$	

Table A2. AC cooling efficiencies.

Template Home	City	AC Cooling Efficiency (e)		
		e_m (°C/kWh)	e_i (°C)	R^2
B2L	Brisbane	1.38	−0.15	0.91
B2M		1.24	−0.11	0.94
B2H		1.03	−0.01	0.95
B6L		1.40	−0.08	0.93
B6M		1.39	−0.08	0.91
B6H		0.90	−0.05	0.88
S2L	Sydney	1.45	−0.46	0.90
S2M		1.24	−0.08	0.96
S2H		0.80	−0.02	0.93
S6L		1.39	−0.11	0.94
S6M		1.36	−0.14	0.89
S6H		0.94	−0.12	0.83
M2L	Melbourne	1.22	−0.31	0.98
M2M		1.22	−0.28	0.98
M2H		0.81	−0.11	0.98
M6L		1.36	−0.41	0.97
M6M		1.31	−0.22	0.97
M6H		0.89	−0.17	0.93
A2L	Adelaide	1.41	−1.10	0.93
A2M		1.16	−0.25	0.97
A2H		0.81	0.02	0.99
A6L		1.45	−0.65	0.96
A6M		1.37	−0.46	0.94
A6H		0.85	−0.18	0.89

Table A3. Thermal mass charging rates.

Template Home	City	Thermal Mass Charging Rate (c)		
		c_m	c_i (°C)	R^2
B2L	Brisbane	0.78	0.06	0.91
B2M		0.32	0.39	0.82
B2H		0.40	0.15	0.86
B6L		0.90	0.07	0.99
B6M		0.46	0.44	0.83
B6H		0.60	0.20	0.88
S2L	Sydney	0.50	0.59	0.95
S2M		0.40	0.31	0.94
S2H		0.35	0.27	0.69
S6L		0.76	0.32	0.93
S6M		0.48	0.54	0.81
S6H		0.53	0.30	0.81

Table A3. *Cont.*

Template Home	City	Thermal Mass Charging Rate (c)		
		c_m	c_i (°C)	R^2
M2L	Melbourne	0.53	0.38	0.99
M2M		0.41	0.14	0.96
M2H		0.36	0.09	0.87
M6L		0.62	0.39	0.93
M6M		0.50	0.32	0.94
M6H		0.27	0.37	0.80
A2L	Adelaide	0.55	0.70	0.97
A2M		0.50	−0.34	0.95
A2H		0.63	−0.70	0.91
A6L		0.77	−0.61	0.94
A6M		0.62	−0.27	0.90
A6H		0.82	−1.52	0.90

Table A4. Thermal mass fast discharging rates.

Template Home	City	Thermal Mass Fast Discharging Rate (d^F)		
		d_m^F	d_i^F (°C)	R^2
B2L	Brisbane	0.53	0.24	0.86
B2M		0.58	0.10	0.84
B2H		0.67	0.07	0.81
B6L		0.74	0.12	0.90
B6M		0.68	0.10	0.87
B6H		0.67	0.06	0.88
S2L	Sydney	0.62	0.02	0.92
S2M		0.63	0.09	0.95
S2H		0.67	0.07	0.87
S6L		0.67	0.29	0.90
S6M		0.75	0.06	0.93
S6H		0.74	0.00	0.88
M2L	Melbourne	0.76	−0.21	0.97
M2M		0.63	−0.09	0.95
M2H		0.75	−0.15	0.97
M6L		0.87	−0.31	0.97
M6M		0.81	−0.14	0.97
M6H		0.73	−0.12	0.85
A2L	Adelaide	0.86	−1.05	0.93
A2M		0.71	−0.44	0.90
A2H		0.79	−0.41	0.97
A6L		0.95	−1.11	0.96
A6M		0.80	−0.45	0.92
A6H		0.85	−0.73	0.87

Table A5. Thermal mass slow discharging rates.

Template Home	City	Thermal Mass Slow Discharging Rate (d^S)		
		d_m^S	d_i^S (°C)	R^2
B2L	Brisbane	0.92	−0.04	0.99
B2M		0.85	0.00	0.97
B2H		0.90	−0.03	0.97
B6L		0.96	−0.04	0.99
B6M		0.92	−0.01	0.98
B6H		0.95	−0.04	0.98
S2L	Sydney	0.91	−0.01	0.99
S2M		0.82	0.03	0.98
S2H		0.94	−0.04	0.98
S6L		0.96	−0.03	1.00
S6M		0.92	0.00	0.99
S6H		0.98	−0.06	0.99
M2L	Melbourne	0.86	0.00	0.99
M2M		0.84	−0.04	0.98
M2H		0.94	−0.05	1.00
M6L		0.93	0.02	1.00
M6M		0.92	−0.04	1.00
M6H		0.97	−0.06	1.00
A2L	Adelaide	0.88	0.05	0.99
A2M		0.87	−0.04	0.98
A2H		0.96	−0.08	0.99
A6L		0.95	0.01	1.00
A6M		0.90	−0.02	0.99
A6H		0.97	−0.06	1.00

References

1. International Energy Association. IEA PVPS Snapshot. 2020. Available online: https://iea-pvps.org/snapshot-reports/snapshot-2020/ (accessed on 5 July 2022).
2. Australian Energy Market Operator. Advice to Commonwealth Government on Dispatchable Capability. 2017. Available online: https://www.aemo.com.au/-/media/Files/Media_Centre/2017/Advice-To-Commonwealth-Government-On-Dispatchable-Capability.PDF (accessed on 5 July 2022).
3. Australian Energy Market Operator. Renewable Integration Study: Stage 1 Report. 2020. Available online: https://aemo.com.au/-/media/files/major-publications/ris/2020/renewable-integration-study-stage-1.pdf?la=en (accessed on 5 July 2022).
4. Centre for Energy and Environmental Markets, University of New South Wales. Voltage Analysis of the LV Distribution Network in the Australian National Electricity Market. 2020. Available online: https://prod-energycouncil.energy.slicedtech.com.au/lv-voltage-report (accessed on 5 July 2022).
5. International Renewable Energy Agency. Future of Solar Photovoltaic. 2019. Available online: https://www.irena.org/-/media/Files/IRENA/Agency/Publication/2019/Nov/IRENA_Future_of_Solar_PV_2019.pdf (accessed on 8 July 2022).
6. Distributed Energy Resources. 2018. Available online: https://arena.gov.au/funding/distributed-energy-resources/ (accessed on 8 July 2022).
7. Olsthoorn, D.; Haghighat, F.; Moreau, A.; Lacroix, G. Abilities and limitations of thermal mass activation for thermal comfort, peak shifting and shaving: A review. *Build. Environ.* **2017**, *118*, 113–127. [CrossRef]
8. Roberts, M.B.; Bruce, A.; MacGill, I. Impact of shared battery energy storage systems on photovoltaic self-consumption and electricity bills in apartment buildings. *Appl. Energy* **2019**, *245*, 78–95. [CrossRef]

9. Keeney, K.R.; Braun, J.E. *Application of Building Precooling to Reduce Peak Cooling Requirements*; ASHRAE Transactions: Atlanta, GA, USA, 1997; Volume 103, pp. 463–469.
10. Rabl, A.; Norford, L. Peak Load Reduction by Preconditioning Buildings at Night. *Int. J. Energy Res.* **1991**, *15*, 781–798. [CrossRef]
11. Braun, J.E. Load control using building thermal mass. *J. Sol. Energy Eng.* **2003**, *125*, 292–301. [CrossRef]
12. Lee, K.H.; Braun, J.E. Model-based demand-limiting control of building thermal mass. *Build. Environ.* **2008**, *43*, 1633–1646. [CrossRef]
13. Yin, R.; Xu, P.; Piette, M.A.; Kiliccote, S. Study on Auto-DR and pre-cooling of commercial buildings with thermal mass in California. *Energy Build.* **2010**, *42*, 967–975. [CrossRef]
14. Rijksen, D.; Wisse, C.; van Schijndel, A. Reducing peak requirements for cooling by using thermally activated building systems. *Energy Build.* **2010**, *42*, 298–304. [CrossRef]
15. Xu, P.; Haves, P.; Piette, M.A. *Peak Demand Reduction from Pre-Cooling with Zone Temperature Reset in an Office Building*; Purdue University: Purdue, IN, USA, 2006.
16. Turner, W.; Walker, I.; Roux, J. Peak load reductions: Electric load shifting with mechanical pre-cooling of residential buildings with low thermal mass. *Energy* **2015**, *82*, 1057–1067. [CrossRef]
17. Ramos, J.S.; Moreno, M.P.; Delgado, M.G.; Domínguez, S.Á.; Cabeza, L.F. Potential of energy flexible buildings: Evaluation of DSM strategies using building thermal mass. *Energy Build.* **2019**, *203*, 109442. [CrossRef]
18. Hu, M.; Xiao, F.; Wang, L. Investigation of demand response potentials of residential air conditioners in smart grids using grey-box room thermal model. *Appl. Energy* **2017**, *207*, 324–335. [CrossRef]
19. Korkas, C.D.; Baldi, S.; Michailidis, I.; Kosmatopoulos, E.B. Intelligent energy and thermal comfort management in grid-connected microgrids with heterogeneous occupancy schedule. *Appl. Energy* **2015**, *149*, 194–203. [CrossRef]
20. O'Shaughnessy, E.; Cutler, D.; Ardani, K.; Margolis, R. Solar plus: Optimization of distributed solar PV through battery storage and dispatchable load in residential buildings. *Appl. Energy* **2018**, *213*, 11–21. [CrossRef]
21. Nelson, J.; Johnson, N.G.; Chinimilli, P.T.; Zhang, W. Residential cooling using separated and coupled precooling and thermal energy storage strategies. *Appl. Energy* **2019**, *252*, 113414. [CrossRef]
22. Ice Energy Brings the Deep Freeze to U.S. Energy Storage. 2019. Available online: https://pv-magazine-usa.com/2019/02/13/ice-energy-brings-the-deep-freeze-to-u-s-energy-storage/ (accessed on 8 July 2022).
23. Saurav, K.; Bansal, H.; Nawhal, M.; Chandan, V.; Arya, V. Minimizing energy costs of commercial buildings in developing countries. In Proceedings of the 2016 IEEE International Conference on Smart Grid Communications (SmartGridComm), Sydney, Australia, 6–9 November 2016; pp. 637–642.
24. Arababadi, R.; Parrish, K. *Reducing the Need for Electrical Storage by Coupling Solar PVs and Precooling in Three Residential Building Types in the Phoenix Climate*; ASHRAE Transactions: Atlanta, GA, USA, 2017; Volume 123.
25. Romaní, J.; Belusko, M.; Alemu, A.; Cabeza, L.F.; de Gracia, A.; Bruno, F. Control concepts of a radiant wall working as thermal energy storage for peak load shifting of a heat pump coupled to a PV array. *Renew. Energy* **2018**, *118*, 489–501. [CrossRef]
26. Seem, J.E. *Modeling of Heat Transfer in Buildings*; The University of Wisconsin-Madison: Madison, WI, USA, 1987.
27. Romaní, J.; Belusko, M.; Alemu, A.; Cabeza, L.F.; de Gracia, A.; Bruno, F. Optimization of deterministic controls for a cooling radiant wall coupled to a PV array. *Appl. Energy* **2018**, *229*, 1103–1110. [CrossRef]
28. Calero, I.; Cañizares, C.A.; Bhattacharya, K.; Baldick, R. *Duck-Curve Mitigation in Power Grids with High Penetration of PV Generation*; IEEE Transactions on Smart Grid: Piscataway, NJ, USA, 2021; Volume 13, pp. 314–329.
29. Smart Residential Load Simulator. 2021. Available online: https://uwaterloo.ca/power-energy-systems-group/downloads/smart-residential-load-simulator-srls (accessed on 15 September 2022).
30. Wang, H.; Good, N.; Mancarella, P. Modelling and valuing multi-energy flexibility from community energy systems. In *2017 Australasian Universities Power Engineering Conference (AUPEC)*; IEEE: Piscataway, NJ, USA, 2017.
31. Perez, K.X.; Baldea, M.; Edgar, T.F. Integrated HVAC management and optimal scheduling of smart appliances for community peak load reduction. *Energy Build.* **2016**, *123*, 34–40. [CrossRef]
32. AccuRate: Helping Designers Deliver Energy Efficient Homes. 2020. Available online: https://www.csiro.au/en/Research/EF/Areas/Grids-and-storage/Intelligent-systems/AccuRate (accessed on 15 September 2022).
33. Nationwide House Energy Rating Scheme. 2020. Available online: https://www.nathers.gov.au/ (accessed on 15 September 2022).
34. A Validation of the AccuRATE Simulation Engine Using BESTEST. 2004. Available online: https://www.nathers.gov.au/sites/default/files/Validation%2520of%2520the%2520AccuRate%2520Simulation%2520Engine%2520Using%2520BESTEST_0.pdf (accessed on 15 September 2022).
35. Judkoff, R.; Neymark, J. *International Energy Agency Building Energy Simulation Test (BESTEST) and Diagnostic Method*; National Renewable Energy Lab. (NREL): Golden, CO, USA, 1995.
36. Household Census Data. 2021. Available online: https://quickstats.censusdata.abs.gov.au/census_services/getproduct/census/2016/quickstat/1GSYD?opendocument (accessed on 22 July 2022).
37. NatHERS Administrator. *Nationwide House Energy Rating Scheme (NatHERS)—Software Accreditation Protocol*; Department of Environment and Energy: Canberra, Australia, 2012.
38. Law, A. Building Evaluation: The decay Method as an Evaluation Tool for Analysing Thermal Performance. Ph.D. Thesis, RMIT University, Melbourne, VIC, Australia, 2018.
39. Guideline, A. *Measurement of Energy, Demand, and Water Savings*; ASHRAE Guidel: Atlanta, GA, USA, 2014; Volume 4, pp. 1–150.